Computational Materials Science 187 (2021) 110058

Contents lists available at ScienceDirect

Computational Materials Science

journal homepage: www.elsevier.com/locate/commatsci

First-principles study of tensile and shear strength of Fe-Al and α-AlFeSi intermetallic compound interfaces

Muhammad Zeeshan Khalid [a,b,*], Jesper Friis [c,d], Per Harald Ninive [a], Knut Marthinsen [b], Are Strandlie [a]

[a] Department of Manufacturing and Civil Engineering, Norwegian University of Science and Technology, Gjøvik 2815, Norway
[b] Department of Materials Science and Engineering, Norwegian University of Science and Technology (NTNU), Norway
[c] SINTEF Industry, Trondheim, Norway
[d] Department of Physics, Norwegian University of Science and Technology, Trondheim, Norway

ARTICLE INFO

Keywords:
Intermetallics
Interfacial properties
UBER
First-principles calculations

ABSTRACT

First-principles virtual tensile and shear strength calculations have been performed on the Fe_2Al_5// Fe_4Al_{13} and α-AlFeSi// Fe_4Al_{13} interfaces. The Fast Inertial Relaxation Engine (FIRE) algorithm is used for optimizing these complex Intermetallic Compound (IMC) interface structures. To characterize the virtual tensile strength, an extended generalized Universal Binding Energy Relation (UBER) was used to fit the energy-displacement data. The virtual tensile strength was evaluated with the Rigid Grain Shift (RGS) methodology without atomic relaxations during tensile displacement and with RGS+relaxation with atomic relaxations. All calculated values for IMC//IMC interfaces in this study are compared with pure Al//Fe and Al//IMCs [1] interfaces to identify the role of IMCs at aluminum-steel joints.

1. Introduction

Combining aluminum and steel is becoming increasingly popular in tailored applications including light-weight and strength in complex structures. At the aluminium/steel joint, a micrometer thick layer of Al-Fe intermetallic compounds (IMCs) is typically formed [2]. The presence of these compounds at the joint influences the mechanical properties of the joint. The most common IMCs found at aluminum and steel joints are Fe_2Al_5 (η) and Fe_4Al_{13} (θ) [3–5]. However, the formation of these compounds largely depends on the chemical composition of the alloys and temperature reached during the joining or post-treatment [3,5].

Since commercial Al-alloys always contain some Si and Fe, Al-Fe-Si phases have also been observed at such joints [6,7]. The potential presence of Fe-Al-Si IMCs at the joint depends on the composition of the aluminum alloys, typically seen in 3xxx, 6xxx and foundry alloys. There have been several studies of the thermodynamic and mechanical properties of Fe-Al and Al-Fe-Si systems [8–11].

Most of the investigations of the Fe-Al and Al-Fe-Si IMCs have mainly been limited to the bulk structural and mechanical properties. For example, Liu et al. [10] studied the electronic and mechanical properties of Fe-Al binary compounds by ab initio methods and found Fe_2Al_5 as the thermodynamically most stable of all Fe-Al IMCs. Zhang et al. [12] also studied the structural and mechanical properties of Fe-Al compounds by Embedded-Atom Method (EAM)-based simulations. The most commonly observed IMCs for the Al-Fe-Si system are β-AlFeSi and α-AlFeSi, where the β-AlFeSi phase is observed to transform into α-AlFeSi [13]. Several studies have investigated the morphology, contents and transformation kinetics of AlFeSi IMCs [14,13,15]. However, according to our best knowledge, so far nobody has explored the interfacial characteristics of these IMC//IMC interface structures.

This work is a follow-up of a comprehensive computational investigation for understanding the role of observed IMCs on the joint strengths of AA6082 and IF steel [5]. The first of its studies, that of the interfaces Al//Fe_4Al_{13} and Al//α-AlFeSi has recently been published [1]. We will make a comparison of the present interfaces with the previously published interface structures between Al//IMCs (α-AlFeSi and Fe_4Al_{13}) throughout this paper. In this work, we study the virtual tensile and shear properties of Fe_2Al_5// Fe_4Al_{13} and α-AlFeSi// Fe_4Al_{13} interface structures and they will be referred to as IMC//IMC interfaces for comparison purposes with Al//IMCs in some parts of the paper. These interfaces are more complex than the former ones, which presents a challenging task from developing low-lattice misfit interface structures

* Corresponding author.
E-mail address: zeeshan.khalid039@gmail.com (M.Z. Khalid).

https://doi.org/10.1016/j.commatsci.2020.110058
Received 26 March 2020; Received in revised form 7 September 2020; Accepted 8 September 2020
Available online 5 October 2020

Table 1
Lattice constants of the Al, Fe_4Al_{13} and b.c.c. α-AlFeSi phases, as calculated in this work and from literature.

Compound	Space group	a (Å)	b (Å)	c (Å)	Angle
Fe_2Al_5		7.418	6.428	4.103	
		7.466 [10]	6.181 [10]	4.808 [10]	$\alpha = \beta = \gamma =$ 90°
		7.622 [12]	6.323 [12]	4.178 [12]	
Fe_4Al_{13}	C2/m	15.49	8.08	12.48	
		15.532 [10]	8.010 [10]	12.398 [10]	$\alpha = 90°, \beta =$ 107.7°
		15.069 [12]	7.864 [12]	12.083 [12]	$\gamma = 90°$
		15.49 [20]	8.083 [20]	12.476 [20]	
α-AlFeSi	Im3	12.69	12.69	12.69	
		12.56 [20]	12.56 [20]	12.56 [20]	$\alpha = \beta = \gamma =$ 90°
		12.589 [21]	12.589 [21]	12.589 [21]	

Table 3
Calculated work of separation of bulk IMCs and interface structures.

	Work of Separation (J/m^2)		
	This work (unstrained)	This work (strained)	others
Fe_4Al_{13}			
(100)	4.46		
(1-1-1)	2.50	4.14	
(10-1)	–		3.17[a]
α-AlFeSi			
(1-11)	3.36	2.33	
(001)	–		2.90[a]
Fe_2Al_5			
(-1-20)	4.33	3.94	
(0-20)			5.54[b]
α-AlFeSi// Fe_4Al_{13}	–	2.95	2.26[a], –
Fe_2Al_5 // Fe_4Al_{13}	–	3.21	–
Al//α-AlFeSi	–	–	2.26[a]
Al// Fe_4Al_{13}	–	–	2.21[a]
Al// Fe	–	–	5.84[c], 3.11[d]

[a] [1].
[b] [22].
[c] [32].
[d] [30].

to the optimization and calculations of mechanical properties of these structures. Despite these challenges, it is still pivotal to study the role of these interfaces to better understand the IMCs role at the aluminum-steel joints. It is worth mentioning that this study is performed without considering any crystallographic defects. Moreover, low lattice misfit and relatively small interface unit cell sizes were set to be the selection criteria for these complex IMC//IMC interfaces. Thus, mechanical properties calculated in this work are over-estimated, but comparison with other Fe-Al interface structures under similar constraints and assumptions is still believed to provide important insights about the mechanical performance of these IMCs.

2. Methods

2.1. Computational method

The atomistic simulations were performed with density functional theory implemented in the Vienna Ab-initio Simulation Package (VASP) [16]. The exchange–correlation energy was evaluated using the Generalized Gradient Approximation (GGA) by Perdew, Burke and Ernzerhof (PBE) [17] and with the Projector Augmented Wave (PAW) [18] method for the electron–ion interaction, using standard Al, Fe and Si potentials with three, eight, and four valence electrons, respectively. The k-point integration was performed by using a Monkhorst-Pack grid with $2 \times 2 \times 1$ for α-AlFeSi// Fe_4Al_{13} and $3 \times 3 \times 1$ for Fe_4Al_{13}// Fe_2Al_5 interfaces with a smearing width of 0.2 eV for the first-order Meth-Fessel-Paxton smearing scheme [19]. The plane-wave cut-off energy was set to at least 450 eV in all calculations to ensure that total energies are converged with inaccuracies of less than a few meV/atom. The interface energies were converged to a precision of 1 mJ/m^2 with these defined input parameters.

2.2. Interface models

Due to the large unit cell size and low symmetry of Fe_4Al_{13} (101 atoms, space group 12), α-AlFeSi (138 atoms, space group 204) and Fe_2Al_5 (14 atoms, space group 65), it is extremely challenging to build a representative interface model which has low lattice misfit and contains a low number of atoms. The interface structures are built using a face-to-face matching technique. The theoretical background of this technique can be found in the literature [22]. For the building of an interface structure, bulk Fe_4Al_{13} and α-AlFeSi atomic positions were taken from the study published by Liu et al. [20]. Table 1 lists the relaxed calculated lattice constants of the IMCs, which are also compared with other published results. The calculated values show consistent agreement with other studies. These values were used further for the building of interface structures.

The interface building process started by considering the relaxed equilibrium structures for all IMC phases. The relaxed lattice constants are given in Table 1. The supercell for the interface structures is created by defining two slabs (defined by $\mathbf{u}_1$, $\mathbf{v}_1$, $\mathbf{w}_1$ and $\mathbf{u}_2$, $\mathbf{v}_2$, $\mathbf{w}_2$, respectively cf. Fig. 6) with minimal lateral misfit in the u-v-plane. Since we added vacuum along the **w** direction, we do not require $\mathbf{w}_1$ and $\mathbf{w}_2$ as lattice vectors. To perfectly match the slabs laterally, each of the two slabs were strained equally (in magnitude, but with opposite sign) according to the following relations:

Table 2
The ORs and lattice misfit for the IMC// IMC interface structures. The indices m_1, m_2, m_3 and n_1, n_2, n_3 defines the lattice vectors **u**, **v**, **w** for each of the two sub-slabs. 'length' is the length of the corresponding lattice vector and 'angle' is the angle between the **u** and **v** directions in respective sub-slab. 'strain' is the strain along the **u** and **v** direction, respectively (equal in magnitude for both slabs) and 'Interface length' is the final length of the matched interface structures.

Interface	**d**	m_1	m_2	m_3	length (Å)	angle	n_1	n_2	n_3	length(Å)	angle	strain (%)	Interface length (Å)
Fe_4Al_{13}// Fe_2Al_5	**u**	0	0	1	12.42		0	0	−3	12.29		1.06	12.355
	v	0	−2	0	16.05	90.0°	2	−1	0	16.14	90.0°	0.56	16.092
	w	1	0	0	11.998		−1	−2	0	12.11		–	–
α-AlFeSi// Fe_4Al_{13}	**u**	1	2	1	17.43		1	1	0	17.76		1.89	17.594
	v	−1	−1	0	17.47	121.5°	0	−1	1	17.76	121.5°	1.66	17.615
	w	1	−1	1	10.76		1	−1	−1	12.60		–	–

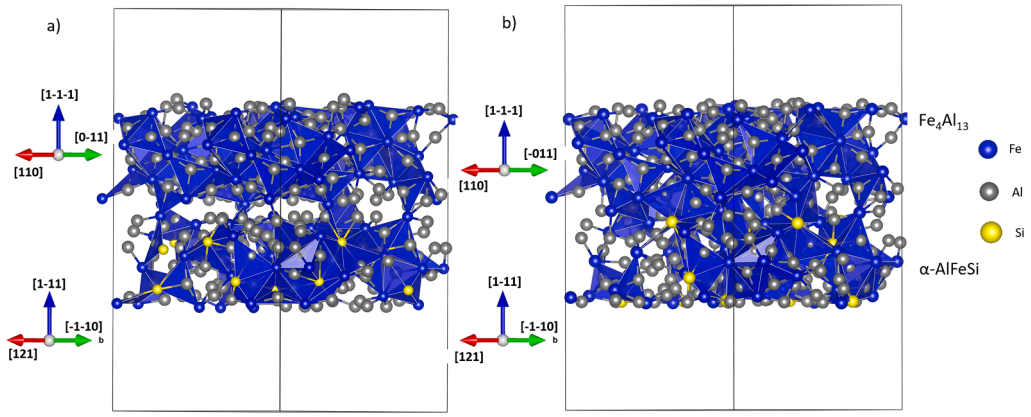

Fig. 1. The interface structures between α-AlFeSi// Fe_4Al_{13}, (a) un-relaxed and (b) DFT-relaxed.

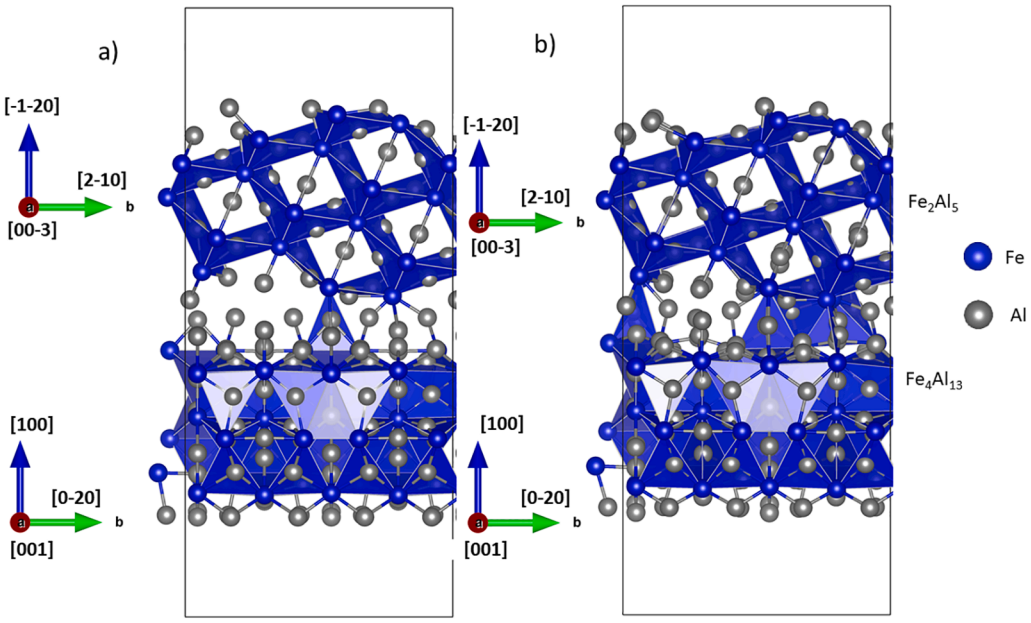

Fig. 2. The interface structures between Fe_2Al_5// Fe_4Al_{13}, (a) un-relaxed and (b) DFT-relaxed.

$$\epsilon_u = \frac{\|\mathbf{u}_2| - |\mathbf{u}_1\|}{\|\mathbf{u}_1| + |\mathbf{u}_2\|} \tag{1}$$

$$\epsilon_v = \frac{\|\mathbf{v}_2| - |\mathbf{v}_1\|}{\|\mathbf{v}_1| + |\mathbf{v}_2\|} \tag{2}$$

Moreover, due to the different symmetry of the IMC slabs, the angle between **u** and **v** may also differ, which is accounted for by using von Misses strain. For simplicity (or rather efficiency), the interfaces are developed by minimizing the strain given in Eqs. (1) and (2). Table 2 lists the supercell dimensions along u, v and w directions of individual IMC phases before matching and introduced lattice misfit strain as a result of interface matching. The final supercell dimension for the Fe_2Al_5// Fe_4Al_{13} interface along the u direction is 12.355 Å and 16.092 Å along the v direction. Comparing these values with the individual bulk phases in Table 3, it can be seen that bulk IMC phases have been compressed/stretched equally to match at the interface.

The effect of strain on the work of separation is discussed in the subsection 3.1. During the optimization process atoms were allowed to relax along all direction to find the minimum energy configuration. However, during the tensile testing, the top two layers were fixed during tensile elongation (See subsection 3.2 for more details).

To reduce the computational cost and avoid the periodic interaction between two artificial interfaces, a vacuum layer of >10 Å was added along the normal direction of the interface. Besides, to ensure the bulk-like interior of phases, a bulk size of >10 Å was selected for both bulk phases of the interface structures. Figs. 1 and 2 show un-relaxed and DFT-relaxed Orientation Relationships (ORs) and atomic configurations of the Fe_2Al_5// Fe_4Al_{13} and α-AlFeSi// Fe_4Al_{13} interface structures. Table 2 lists the OR and lattice misfits for both interface structures.

Considering the complex nature of these IMCs, we made some approximations about the selection of interface structures to simplify and reduce the computational cost. The minimum interface energy occurs when close-packed or nearly close-packed atom rows match at the interface [23]. For this reason, interface structures were selected where nearly close-packed planes of both IMCs meet at the interface.

2.3. Optimization method

A major challenge is to relax the atom positions to minimize the total energy of these complex interface structures. To optimize these interfaces a force-based optimization method, FIRE was used [24]. FIRE was found to be surprisingly fast and efficient for the optimization of these complex interface structures. Since these interfaces have large numbers of degrees of freedom, finding minimum energy paths are

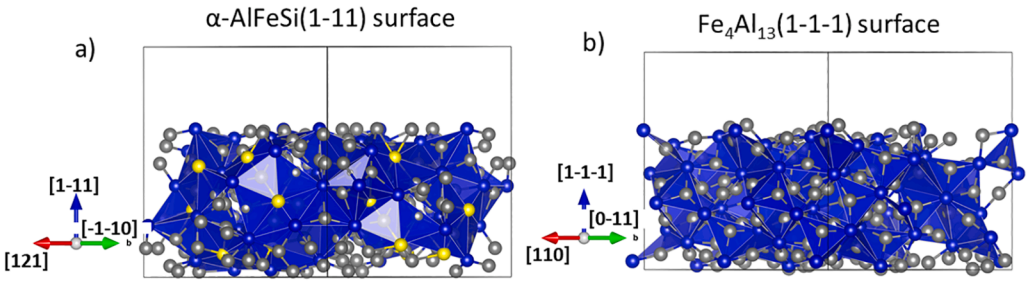

Fig. 3. The surfaces of (a) α-AlFeSi(1–11) and (b) Fe_4Al_{13} (1-1-1).

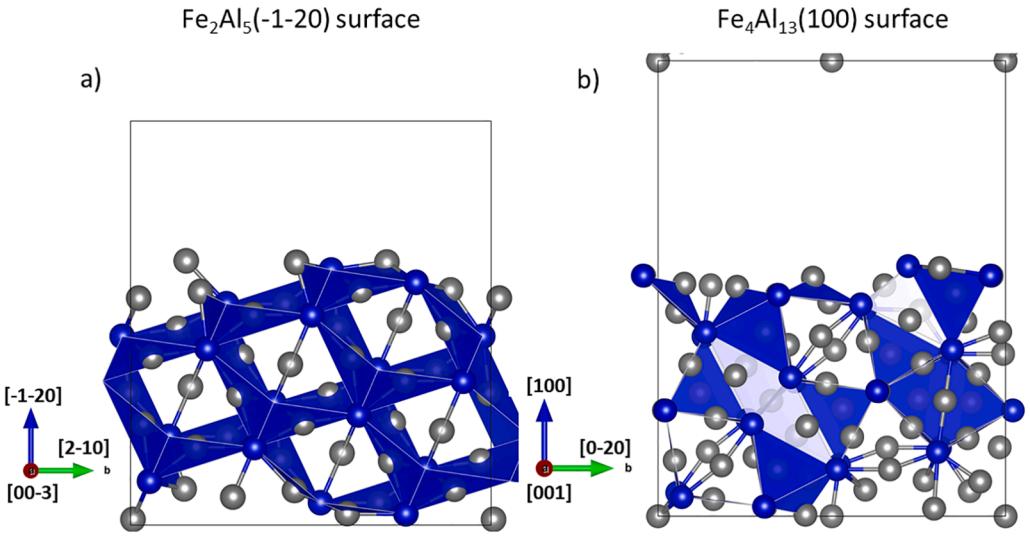

Fig. 4. The surfaces of (a) Fe_2Al_5 (1-20) and (b) Fe_4Al_{13} (100).

computationally expensive. FIRE was in particular found to be successful in finding minimum energy paths due to its ability to stop and steer based on the information of force and velocity. A more detailed description of this method can be found in the literature [24], together with how it is implemented in VASP [25,26]. By using the FIRE optimization scheme, the average force per atom was reduced to 0.01 eV/Å^2, and total energy changes were converged to 1×10^{-5} eV. However, for the virtual tensile and shear strength calculations, the conjugate gradient optimization method was used to relax the atomic positions by keeping the cell size fixed. Figs. 1b and 2b show the optimized interface structures. It can easily be seen that interfacial atoms move towards each other during the relaxation of atomic positions. This results in higher polyhedral bonding density at the interface as compared to the unrelaxed interface structure (Figs. 1a and 2a), which is empirical evidence for the effectiveness of the FIRE optimization technique.

3. Bulk and interface strengths

3.1. Ideal work of separation

In this part, we calculate the work of separation of bulk IMCs surfaces which is the energy needed to form two free surfaces by breaking the interfacial bonds [27,28]. It is also referred to as the "Ideal work of separation". In the present study, Ideal work of separation of bulk IMCs are calculated according to

$$W_{sep} = \frac{E_a^{tot} + E_b^{tot} - E_{ab}^{tot}}{A} \tag{3}$$

where A is the surface area of the supercell, E_{ab}^{tot} is the total energy of an IMC supercell containing multilayered slabs, and E_a and E_b represent the total energies of the same IMC supercell containing a single slab, separated by a vacuum layer. Figs. 3 and 4 show the surfaces of the bulk IMC supercells considered in this study. To make consistent comparisons with bulk and interface structures, the same ORs were used for bulk IMCs as for the interfaces. When it comes to the choice of termination, we used the same assumption as we used for the interface structures of a close-packed plane. Furthermore, different planes were considered to calculate W_{sep} values to clarify the anisotropic behavior of these phases. In addition, detailed comparative analyses based on the calculated W_{sep} values were carried out between bulk IMCs, IMC//IMC, Al//IMCs, and pure Al//Fe interfaces to designate the bonding nature and mechanical response of the IMCs.

The calculated W_{sep} for bulk and interface structures are summarized in Table 3 along with other theoretical results from literature. The results indicate that the Fe_2Al_5 IMC phase has the highest W_{sep} of all the IMCs considered in this study. The highest value is reported for Fe_2Al_5 (0-20) plane (5.54 J/m^2). The Fe_4Al_{13} phase shows contrasting results with the highest value reported to be 4.46 J/m^2 along the (100) plane and lowest 2.50 J/m^2 along the (1-1-1) plane. The significant difference in the calculated values shows the highly anisotropic behavior of the Fe_4Al_{13} phase. IMCs with highly anisotropic nature are more prone to introduce micro-cracks. This is consistent with the experimental study by Liu et al. [29]. They observed micro-cracks in the Al-rich IMCs by explosive Fe-Al welding. Our previous study [1], also reported a charge depletion region in the Fe_4Al_{13} (10-1) plane with the lowest value reported to be 1.15 J/m^2. Comparisons of bulk with interfacial structures indicate higher W_{sep} values for the former. This indicates that the interface structures could be the weaker link in the overall IMCs structure and fracture could initiate from the interfacial region.

Other comparisons of present IMC//IMC interfaces with Al//IMCs

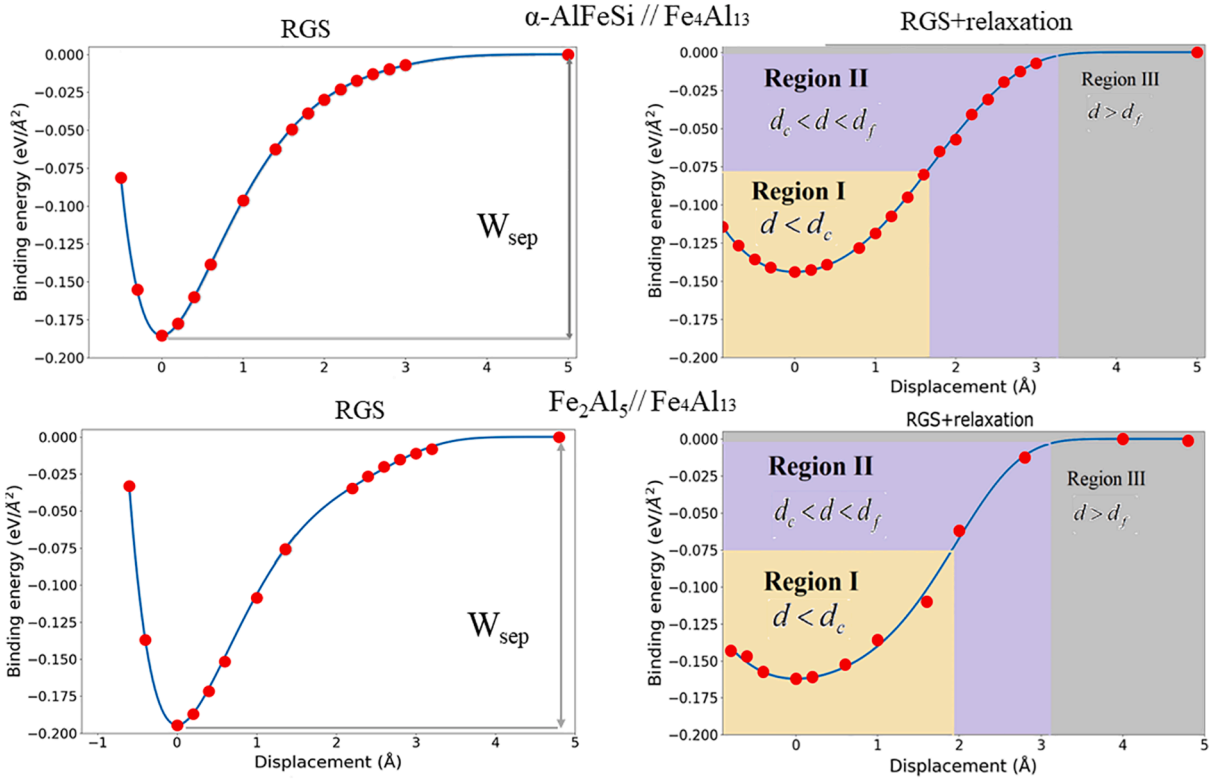

Fig. 5. Energy-displacement curves of the RGS and RGS+relaxation virtual tensile strength calculations for α-AlFeSi// Fe_4Al_{13} and Fe_2Al_5// Fe_4Al_{13} interface structures. Red points show the values from DFT calculations and the blue solid line is the fitted curve..

[1] and pure Al//Fe [11,30] show that the Al//IMCs interfaces have lower values of W_{sep} than the IMC//IMC interfaces, which indicates that IMCs develop stronger bonds with each other than with the Al lattice. However, IMC interfaces still show lower W_{sep} values compared to the pure Al//Fe interfaces, which give an indication of the deteriorating effect of the present IMCs at the aluminum and steel joint. This conclusion is consistent with an experimental study reported by Qian et al. [31]. They reported that Fe_2Al_5 and Fe_4Al_{13} significantly deteriorated the mechanical properties of Al-Fe clad materials.

In order to find the strain energy contribution to the work of separation, we performed additional calculations by considering strained (according to the interface structure) bulk IMC structures in the interface cell. Table 3 lists the work of separation for the unstrained (relaxed) and strained bulk structures. The work of separation value was reduced for both Fe_4Al_{13} and Fe_2Al_5 structures. Even though, both structures were strained equally, Fe_2Al_5 showed a slightly higher effect of energy on work of separation than the Fe_4Al_{13}. On the other hand, α-AlFeSi showed the highest effect of strain on the work of separation.

3.2. Virtual tensile test calculations

For the virtual tensile strength calculations, two types of approaches were adopted. In the first approach, interface structures were separated by adding a vacuum layer at the interface, and static calculations were performed without any atomic relaxations. This approach is denoted the Rigid Grain Shift (RGS) methodology [33]. In the second approach, interface structures were initially separated in the same way as for RGS, then allowing for relaxation of atomic positions to minimize the total energy. Therefore, this approach is denoted RGS+relaxation [34–36]. The energy calculated from these approaches were fitted by a generalized version of the Universal Binding Energy Relation (UBER) proposed by Rose et al. [37]. The details of this methodology can be found in the following literature [1,36].

3.3. Virtual tensile strengths

As discussed in the previous subsection, two types of calculations were performed for characterizing the virtual tensile strength, i.e, RGS and RGS+relaxation. These virtual tensile tests result in energy-displacement curves. For both interface structures, the results of these virtual tensile tests are shown in Fig. 5 for the RGS and RGS+relaxation approaches, respectively. The value of the binding energy increases with increasing tensile displacement. W_{sep} is defined as the energy required to separate an interface structure into two rigid bulk surfaces ($-E_b(0) = W_{sep}$) [38]. Table 4 lists the W_{sep} values for both interface structures. W_{sep} for the Fe_2Al_5// Fe_4Al_{13} interface is higher (0.20 eV/Å^2 = 3.21 J/m^2) than for the α-AlFeSi// Fe_4Al_{13} interface structure (0.184 eV/Å^2 = 2.95 J/m^2). Table 4 also lists σ_{UTS} for both interface structures. The α-AlFeSi// Fe_4Al_{13} interface shows an almost equal σ_{UTS} (17.79 GPa) to that of the Fe_2Al_5// Fe_4Al_{13} interface (17.60 GPa).

The RGS+relaxation approach provides an opportunity of finding an elastic limit and allows an exploration of the theoretical brittleness and

Table 4
Calculated ultimate tensile strengths of Fe_2Al_5// Fe_4Al_{13} and α-AlFeSi// Fe_4Al_{13} interface structures.

Structure	σ_{UTS} (RGS) (GPa)	d_c (Å)	d_f (Å)	$d_{instability}$ (Å)	σ_{UTS} (RGS+relaxation) (GPa)	W_{sep} (J/m^2)	W_{ad} (J/m^2)
Fe_2Al_5// Fe_4Al_{13}	17.60	1.97	3.07	1.10	14.48	3.21	2.60
α-AlFeSi// Fe_4Al_{13}	17.79	1.65	3.20	1.55	11.10	2.95	2.31

ductility of the defect free interface structures. The energy-displacement curve obtained from this methodology is less steep than the RGS curve, and it is harder to find the best fit than with the RGS approach. As Rose pointed out, UBER does not describe well the binding energy versus displacement relationship with the RGS+relaxation methodology for tightly bound metals [39]. Higher-order polynomial terms were therefore taken into account to find the best fit. We also performed some virtual compression tests. To find a good fit for the compression/expansion virtual tensile tests, only odd-order polynomial terms were considered. The best fits found for these interfaces are shown in Fig. 5. The minimum value of the binding energy curve defines the work of adhesion W_{ad} in the RGS+relaxation approach, which is defined as the irreversible work required to separate an interface structure into relaxed surfaces [38].

For the RGS+relaxation virtual tensile tests, the energy-displacement curve can be divided into three distinct regions [34,35], as shown with three different colors in Fig. 5. Region I is defined as the elastic region ($d < d_c$), where the crack introduced can potentially be healed during elastic relaxations for smaller displacements. This region is described well by Hooke's law. With an increase in tensile displacement, the nominal value of the binding energy increases until the tensile displacement reaches the critical length d_c, where the structure reaches maximum of its tensile strength which lies beyond the limits of Hook's law. Table 4 lists the values of d_c for both interface structures. The Fe_2Al_5// Fe_4Al_{13} interface has a higher d_c (1.97 Å) than the α-AlFeSi// Fe_4Al_{13} interface (1.65 Å).

Region II is defined as the instability region ($d_c < d < d_f$). In this region, the interface structure is neither able to heal by elastic relaxations nor are the two slabs completely separated into two surfaces. In this region, atoms experience forces from both bulk atoms and try to overcome the energy barrier until the structure is finally separated into two relaxed surfaces at the final fracture length d_f. There is no unique way of determining d_f, but we define the final fracture length as the displacement where the binding energy reaches -0.003 eV/Å^2. The range of the instability region is determined by the difference between d_f and d_c ($d_{\text{instability}} = d_f$-$d_c$). We used this approach consistently for other interfaces [1] to find the relative range of this instability region, which helps in determining the intrinsic brittle/ductile nature of distinct IMCs interfaces. It is important to mention that the calculation and estimation of brittleness/ductility are not defined in the classical sense as relevant for real microstructures and materials, but it is a qualitative comparison between different IMC interfaces indicating the intrinsic brittle/ductile failure mechanism as also discussed in related studies [1,35]. Materials having a short range of their instability regions tend to show a brittle nature, because they overcome the energy barrier for final fracture abruptly. Fe_2Al_5// Fe_4Al_{13} showed lower $d_{instability}$ (1.10 Å) than the α-AlFeSi// Fe_4Al_{13} interface (1.55 Å), which indicates a more brittle nature of the former interface than the latter. However, Al//α-AlFeSi showed the lowest range of instability region (0.86 Å) as reported in the previous work [1]. This indicates that α-AlFeSi acts as more brittle when developing bonds with the pure Al phase than with the Fe_4Al_{13} phase. The weaker bonding between Si and Al atoms has been found to be the main reason for this observation in the same study [1]. To summarize, the Fe_4Al_{13} and Fe_2Al_5 phases are indicated to exhibit a less brittle failure mechanism than the α-AlFeSi IMC.

Region III is defined as the final fracture zone ($d > d_f$), where the interface structures are completely separated into two relaxed surfaces. In this region, bulk surfaces have no bonding at the interfaces, and the bulk IMCs relax independently. For this reason, the curve levels out and the height under the curve relative to the minimum gives converged work of adhesion W_{ad} values. The calculated W_{ad} values are summarized in Table 4. Normally, W_{ad} values follow the same trend as the W_{sep}, i.e. interfaces having higher W_{sep} shows the higher W_{ad}. The same trend can also be seen in the present work.

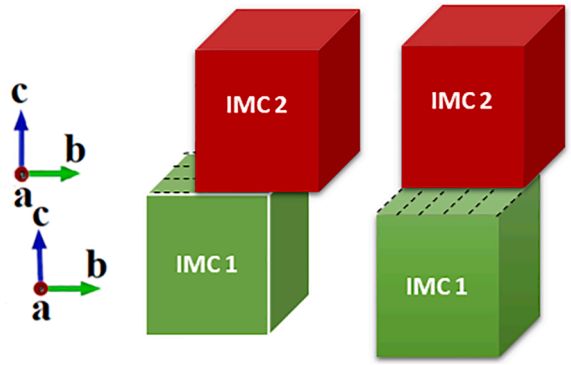

Fig. 6. Schematic illustration of shear direction of IMC//IMC interfaces a) perfect IMC//IMC interface with no shear, b) Shearing along **v** direction, and c) shearing along the **u** direction.

3.4. Tensile strength

Table 4 lists σ_{UTS} for both interface structures. The Fe_2Al_5// Fe_4Al_{13} interface has a higher value of σ_{UTS} than the α-AlFeSi// Fe_4Al_{13} interface structure. Further comparisons of present IMC//IMC interfaces with Al//IMCs [1] indicate that the IMC//IMC have higher tensile strength than the Al//IMCs interfaces. Since these IMCs phases are hard and brittle in nature [10], it is not surprising to find higher tensile strengths for the IMC//IMC interfaces than for the Al//IMCs interfaces. Generally, materials having higher W_{sep} and W_{ad} values have a higher σ_{UTS} value, and the same trend has been found in this study. Comparisons of the W_{sep} values with that of the pure Al// Fe interface [32,30] show that the latter have a higher value of W_{sep} than that of the α-AlFeSi// Fe_4Al_{13} (2.95 J/m^2) and Fe_2Al_5// Fe_4Al_{13} (3.21 J/m^2) interfaces, which indicates that the presence of these IMCs at the aluminium and steel joint have negative effects on the joint strength. However, the Fe_2Al_5 phase has been found less detrimental than the Fe_4Al_{13} and α-AlFeSi phases due to its higher tensile strength [22]. Still the joint strength can not solely be ranked based on the theoretical tensile strength. Current calculations indicate that the presence of Si atoms in α-AlFeSi tends to produce intrinsic brittle failure [1]. Therefore, despite producing higher tensile strength, this phase can be prone to brittle failure.

3.5. Virtual shear strength

To determine the shear strength, Fe_4Al_{13} and α-AlFeSi phases of the interface structures are shifted along **u** and **v** directions as shown in Fig. 6 for the Fe_2Al_5// Fe_4Al_{13} and α-AlFeSi// Fe_4Al_{13} interface structures, respectively. The shear loading for the shear strength calculations is a planar glide of two crystals on top of each other as shown in Fig. 6. The vector directions of **a** and **b** refer to the ORs between the interface structures. During the calculations, atoms were allowed to relax along the normal direction of an interface to remove strain. These calculations result in a energy-displacement curve, which was fitted with a Fourier series,

$$E_s(d) = E_0 + \sum_{n=1}^{\infty}[A_n cos(k_n d) + B_n sin(k_n d)] \tag{4}$$

where d is the shear displacement, and $E_s(d)$ and E_0 are the energy of the displaced and equilibrium ground state structure, respectively. The periodicity of the structure is defined by λ, and therefore $k_n = \frac{2\pi n}{\lambda}$ (See Appendix Table A6 and A7 for the values of the Fourier series coefficients and λ). The shear stress is calculated by differentiating Eq. (4),

$$\gamma_s = \frac{1}{A}\frac{\partial E_s}{\partial d} \tag{5}$$

where A is the unit cell interface area. The first three terms of the Fourier

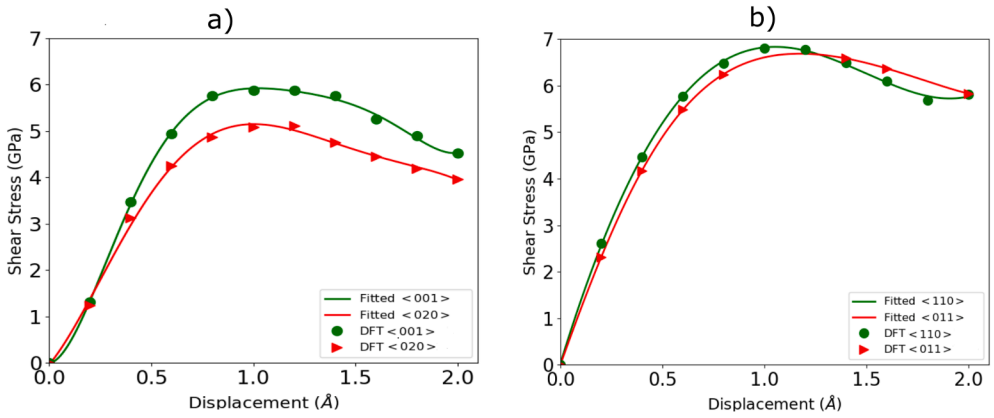

Fig. 7. Fitted shear strength curves of IMC// IMC interfaces between (a) Fe_2Al_5// Fe_4Al_{13}, and (b) α-AlFeSi// Fe_4Al_{13} interface structures.

Table 5
Ideal shear strength of IMC// IMC Interface.

Interface	<001> (GPa)	<020> (GPa)	<110> (GPa)	<011> (GPa)
Fe_2Al_5//Fe_4Al_{13}	5.92	5.15	–	–
α-AlFeSi// Fe_4Al_{13}	–	–	6.81	6.50

series are used in the fit of the energy-displacement curve. Except for a few outliers, the Fourier series fits nicely. The shear stress-displacement curve obtained from Eq. (5) is shown in Fig. 7.

With an increase in shear displacement, the shear stress increases until it reaches a maximum value, and then it starts to decrease again. The shear strength is calculated at the maximum shear value of γ_s. Table 5 lists the shear strength for both interface structures along different slip directions. For the Fe_2Al_5// Fe_4Al_{13} interface, the $< 020 >$ direction show a lower shear strength (5.15 GPa) as compared to the $< 001 >$ slip direction (5.92 GPa). α-AlFeSi// Fe_4Al_{13} shows a higher shear strength than the Fe_2Al_5// Fe_4Al_{13} interface. Moreover, there are no significant differences in shear strength values along $< 110 >$ and $< 011 >$ slip directions. The interfaces studied in this work show comparatively higher shear strengths than for the Al//IMCs interfaces [1].

Overall, these calculations give indications of a higher shear resistance for the α-AlFeSi// Fe_4Al_{13} interface.

4. Discussion

First-principles calculations have been performed to quantify the virtual tensile and shear strengths of the Fe_2Al_5// Fe_4Al_{13} and α-AlFeSi// Fe_4Al_{13} interface structures. These interfaces have been observed during the welding of aluminum and steel using the cold roll-bonded welding technique [5].However, it is challenging experimentally to identify the strength of these interfaces due to the small thickness of the joint and the complex nature of the interface structure. This is why we have to resort to a computational approach as in this work to get some insights into the mechanical behavior of these interfaces, which makes theoretical calculations relevant and important.

The process of theoretical calculations started with the development of representative interface models. Due to the larger unit cell sizes of relevant IMCs, the selection of representative atomic interface structures presents an computational challenge. To address this problem, we relied on the interfaces with the lowest possible lattice misfit strain while keeping the unit cell size of the interfaces within the capabilities of DFT computations and considered densely-packed planes for interface matching using face-to-face matching technique. Moreover, tensile strengths calculated from the RGS+relaxation method depends on the number of crystallographic layers in the system. However, due the large cell sizes of the interface structures it is computationally quite demanding to make an exhaustive investigation of the influence of different numbers of crystallographic layers on the strength results, and this is thus beyond the scope of this paper. Cerny et al. [40] recently studied the effect of cell size on the tensile strength for crystals and interfaces and found the strength decreases steadily with increasing cell size. Therefore, further investigation are needed to find the influence of the number of layers on the strength values for model development using the RGS+relaxation method in future work. The values obtained from the RGS+relaxation method provide qualitative comparative strength values of the IMC//IMC interface as compared to the Al/IMC, IMC//Fe, and pure Al//Fe interfaces. This provides useful insights into the role of different Fe-Al IMCs on the joining of aluminum and steel.

The present first-principles calculations show that the Fe_2Al_5// Fe_4Al_{13} interface exhibit a higher virtual tensile strength but lower shear strength than the α-AlFeSi// Fe_4Al_{13} interface structure. Moreover, bulk calculations of the Fe_4Al_{13} and Fe_2Al_5 IMCs indicate that Fe_2Al_5 is a harder phase than Fe_4Al_{13} [11], while α-AlFeSi is found to be softer than Fe_4Al_{13} and Fe_2Al_5. These results indicate that harder phases develop stronger interfacial bonds. In terms of intrinsic ductility and brittleness, Fe-Al IMCs indicate less brittle nature than the α-AlFeSi phase. However, the α-AlFeSi// Fe_4Al_{13} interface show less intrinsic brittle behaviour than the Fe_2Al_5// Fe_4Al_{13} interface, as indicated by the range of the instability region. Overall, the Al//α-AlFeSi interface shows more intrinsic brittle nature than all the interfaces considered in this study. From the above results, it can be seen that bulk IMCs are harder and stronger than the interface structures. This is why they develop stronger -but weaker than the bulk IMC- interfacial bonds with each other than with the Al lattice. Still, the Fe_2Al_5 phase shows stronger bonding with pure Fe than all the IMCs [22]. Charge density plots studied [1,10,11] indicated the higher charge transfer between the Fe and Al atoms than between the Al-Al, Fe-Fe and Al-Si atoms. This charge transfer results in the stronger bonding between Fe-Al atoms, which furthermore results in the higher strengths for the interfaces and IMCs having a higher number of Fe-Al bonding regions.

Our results hopefully contribute to an improved understanding of the effects Fe_2Al_5, Fe_4Al_{13} and α-AlFeSi IMCs have on the joint strength of aluminum and steel. It should be noted, however, that the strength considerations in this study does not take into account the effects of microstructure features like dislocations, precipitates impurities, grain boundaries) and the effect of temperature on mechanical properties. Thus, it is not straight forward to transfer the conclusions of this work on ideal defect-free structures to real structures in which these lattice defects may completely dominate the failure behavior.

Table A.6
The fitting coefficient values for the α-AlFeSi//Fe_4Al_{13} interface.

Terms	1	5	7	9	11	13
RGS	0.621	0.00035	0.000042	0.00084	0.000018	−0.00054
RGS+relaxation	2.041	0.215	0.310	0.642	0.005	−29.286

Table A.7
The fitting coefficient values for the Fe_2Al_5// Fe_4Al_{13} interface.

Terms	1	5	7	9	11	13	15
RGS	0.646	0.00189	−0.000061	−0.0026	–	–	–
RGS+relaxation	1.906	−0.671	0.224	−0.266	0.230	−0.380	1.156

5. Conclusions

Virtual tensile and shear calculations have been performed for the Fe_2Al_5// Fe_4Al_{13} and α-AlFeSi// Fe_4Al_{13} interface structures to make qualitative comparisons with Fe-Al IMC interfaces. Using a consistent methodology and calculation techniques, virtual tensile and shear strengths were compared for Fe-Al IMC interfaces to determine the role of Fe-Al IMCs on the joining of aluminium and steel.

Virtual tensile calculations were performed using the RGS and RGS+relaxation-based approaches. Virtual tensile strength values calculated with the RGS method show slightly lower σ_{UTS} for the Fe_2Al_5// Fe_4Al_{13} interface (17.60 GPa) than for the α-AlFeSi// Fe_4Al_{13} interface structure (17.79 GPa). However, the RGS approach ignores atomic relaxations during tensile displacement, which leads to over-estimated values for σ_{UTS}. To better understand the fracture mechanism, a RGS+relaxation methodology was performed, indicating a higher σ_{UTS} and more intrinsic brittle nature for Fe_2Al_5// Fe_4Al_{13} (14.48 GPa) than for the Fe_2Al_5// Fe_4Al_{13} interface structure. However, virtual shear strength calculations indicated a higher shear strength for the α-AlFeSi// Fe_4Al_{13} interface as compared to the Fe_2Al_5// Fe_4Al_{13} interface structure. Comparisons of the IMC//IMC studied in this study with the Al// IMCs studied in [1] indicate higher theoretical tensile and shear strengths for the IMC//IMC interfaces than for the Al//IMCs. Moreover, α-AlFeSi tends to show a more intrinsic brittle nature than the Fe-Al IMCs, which is reasoned due to the weaker bonding nature of Si-Al atoms [1].

CRediT authorship contribution statement

Muhammad Zeeshan Khalid: Methodology, Conceptualization, Software, Data curation, Writing - original draft, Visualization, Investigation, Formal analysis, Writing - review & editing, Validation. **Jesper Friis:** Methodology, Software, Data curation, Formal analysis, Supervision, Writing - review & editing, Conceptualization, Validation. **Per Harald Ninive:** Methodology, Software, Supervision, Resources, Writing - review & editing, Validation. **Knut Marthinsen:** Supervision, Project administration, Writing - review & editing, Validation, Formal analysis. **Are Strandlie:** Formal analysis, Supervision, Project administration, Resources, Writing - review & editing, Funding acquisition, Validation.

Declaration of Competing Interest

The authors declare that they have no known competing financial interests or personal relationships that could have appeared to influence the work reported in this paper.

Acknowledgements

The work reported in this paper is based on activities within the centre for research-based innovation SFI Manufacturing in Norway and is partially funded by the Research Council of Norway under contract number 237900. UNINETT Sigma2 AS (The Norwegian Metacenter for High Performance Computing) provided computational resources through Project NN9466K and NN9158K.

Appendix A

See Tables A.6 and A.7.

Appendix B. Supplementary data

Supplementary data associated with this article can be found, in the online version, athttps://doi.org/10.1016/j.commatsci.2020.110058.

References

[1] M.Z. Khalid, J. Friis, P.H. Ninive, K. Marthinsen, A. Strandlie, Ab-initio study of atomic structure and mechanical behaviour of Al/Fe intermetallic interfaces, Computational Materials Science 174 (2020), 109481 .
[2] T. Sakiyama, G. Murayama, Y. Naito, K. Saita, Y. Miyazaki, H. Oikawa, T. Nose, Dissimilar metal joining technologies for steel sheet and aluminum alloy sheet in auto body, Nippon Steel Technical Report 103 (2013) 91–98.
[3] H. Springer, A. Kostka, J. Dos Santos, D. Raabe, Influence of intermetallic phases and kirkendall-porosity on the mechanical properties of joints between steel and aluminium alloys, Materials Science and Engineering: A 528 (2011) 4630–4642.
[4] L. Xu, L. Wang, Y.-C. Chen, J.D. Robson, P.B. Prangnell, Effect of interfacial reaction on the mechanical performance of steel to aluminum dissimilar ultrasonic spot welds, Metallurgical and Materials Transactions A 47 (2016) 334–346.
[5] S.M. Arbo, T. Bergh, H. Solhaug, I. Westermann, B. Holmedal, Influence of thermomechanical processing sequence on properties of AA6082-IF steel cold roll bonded composite sheet, Procedia Manufacturing 15 (2018) 152–160.
[6] S. Kobayashi, T. Yakou, Control of intermetallic compound layers at interface between steel and aluminum by diffusion-treatment, Materials Science and Engineering: A 338 (2002) 44–53.
[7] A. Kurakin, Mechanism of the influence of silicon on the processes of the reaction diffusion of iron in aluminium, Physics of Metals and Metallography (Fiz. Metal. Metalloved.) 30 (1970) 105–110.
[8] L. Amirkhanyan, T. Weissbach, T. Gruber, T. Zienert, O. Fabrichnaya, J. Kortus, Thermodynamic investigation of the τ_4-Al-Fe-Si intermetallic ternary phase: a density-functional theory study, Journal of Alloys and Compounds 598 (2014) 137–141.
[9] T. Klaver, G. Madsen, R. Drautz, A dft study of formation energies of Fe-Zn-Al intermetallics and solutes, Intermetallics 31 (2012) 137–144.
[10] Y. Liu, X. Chong, Y. Jiang, R. Zhou, J. Feng, Mechanical properties and electronic structures of Fe-Al intermetallic, Physica B: Condensed Matter 506 (2017) 1–11.
[11] M.Z. Khalid, J. Friis, P.H. Ninive, K. Marthinsen, A. Strandlie, DFT calculations based insight into bonding character and strength of Fe2Al5 and Fe4Al13 intermetallics at Al-Fe joints, Procedia Manufacturing 15C (2018) 1407–1415.
[12] C.-H. Zhang, S. Huang, J. Shen, N.-X. Chen, Structural and mechanical properties of Fe-Al compounds: an atomistic study by EAM simulation, Intermetallics 52 (2014) 86–91.
[13] H. Becker, T. Bergh, P. Vullum, A. Leineweber, Y. Li, Effect of mn and cooling rates on α-, β- and δ-Al-Fe-Si intermetallic phase formation in a secondary Al-Si alloy, Materialia 5 (2019), 100198 .
[14] N.C. Kuijpers, F.J. Vermolen, K. Vuik, S. van der Zwaag, A model of the β-AlFeSi to α-Al (FeMn) Si transformation in Al-Mg-Si alloys, Materials Transactions 44 (2003) 1448–1456.
[15] J.M. Sanchez, I. Vicario, J. Albizuri, T. Guraya, J.C. Garcia, Phase prediction, microstructure and high hardness of novel light-weight high entropy alloys, Journal of Materials Research and Technology 8 (2019) 795–803.
[16] G. Kresse, J. Furthmüller, Vienna ab-initio simulation package (VASP), Vienna University, Vienna, 2001.

[17] J.P. Perdew, K. Burke, M. Ernzerhof, Generalized gradient approximation made simple, Physical Review Letters 77 (1996) 3865.
[18] P.E. Blöchl, Projector augmented-wave method, Physical Review B 50 (1994) 17953.
[19] H.J. Monkhorst, J.D. Pack, Special points for Brillouin-zone integrations, Physical Review B 13 (1976) 5188.
[20] P. Liu, G. Dunlop, Crystallographic orientation relationships for Al-Fe and Al-Fe-Si precipitates in aluminium, Acta Metallurgica 36 (1988) 1481–1489.
[21] A.M.F. Muggerud, Y. Li, R. Holmestad, Composition and orientation relationships of constituent particles in 3xxx aluminum alloys, Philosophical Magazine 94 (2014) 556–568.
[22] M.Z. Khalid, J. Friis, P.H. Ninive, R.I.G. Marthinsen, Knut, A. Strandlie, First-principles study of tensile and shear strength of an Fe2Al5//Fe interface, 2020 (in preparation).
[23] P. Kelly, M.-X. Zhang, Edge-to-edge matching-the fundamentals, Metallurgical and Materials Transactions A 37 (2006) 833–839.
[24] E. Bitzek, P. Koskinen, F. Gähler, M. Moseler, P. Gumbsch, Structural relaxation made simple, Physical Review Letters 97 (2006), 170201 .
[25] D. Sheppard, R. Terrell, G. Henkelman, Optimization methods for finding minimum energy paths, The Journal of Chemical Physics 128 (2008), 134106 .
[26] D. Sheppard, R. Terrell, G. Henkelman, Force based optimizers, 2008.
[27] S.B. Sinnott, E.C. Dickey, Ceramic/metal interface structures and their relationship to atomic-and meso-scale properties, Materials Science and Engineering: R: Reports 43 (2003) 1–59.
[28] S. Lu, Q.-M. Hu, M.P. Punkkinen, B. Johansson, L. Vitos, First-principles study of fcc-Ag/bcc-Fe interfaces, Physical Review B 87 (2013), 224104 .
[29] W. Liu, J. Ma, M.M. Atabaki, R. Kovacevic, Joining of advanced high-strength steel to AA 6061 alloy by using Fe/Al structural transition joint, Materials & Design 68 (2015) 146–157.
[30] K. Czelej, K.J. Kurzydłowski, Ab initio prediction of strong interfacial bonding in the Fe- Al bimetallic composite system, Scripta Materialia 177 (2020) 162–165.
[31] W. Qian, X.-S. Leng, T.-H. Yang, J.-C. Yan, Effects of Fe-Al intermetallic compounds on interfacial bonding of clad materials, Transactions of Nonferrous Metals Society of China 24 (2014) 279–284.
[32] M.Z. Khalid, J. Friis, P.H. Ninive, K. Marthinsen, A. Strandlie, A first-principles study of the Al (001)/Fe (0–11) Interface, in: Materials Science Forum, volume 941, Trans Tech Publ, pp. 2349–2355.
[33] F. Ehlers, M. Seydou, D. Tingaud, F. Maurel, Y. Charles, S. Queyreau, Ab initio determination of the traction–separation curve for a metal grain boundary: a critical assessment of strategies, Modelling and Simulation in Materials Science and Engineering 24 (2016), 085014 .
[34] D. Zhao, O.M. Løvvik, K. Marthinsen, Y. Li, Segregation of Mg, Cu and their effects on the strength of Al σ5 (210)[001] symmetrical tilt grain boundary, Acta Materialia 145 (2018) 235–246.
[35] P. Lazar, R. Podloucky, Cleavage fracture of a crystal: Density functional theory calculations based on a model which includes structural relaxations, Physical Review B 78 (2008), 104114 .
[36] R. Janisch, N. Ahmed, A. Hartmaier, Ab initio tensile tests of Al bulk crystals and grain boundaries: Universality of mechanical behavior, Physical Review B 81 (2010), 184108 .
[37] J.H. Rose, J.R. Smith, J. Ferrante, Universal features of bonding in metals, Physical Review B 28 (1983) 1835.
[38] R. Yang, S. Tanaka, M. Kohyama*, First-principles study on the tensile strength and fracture of the Al-terminated stoichiometric α-Al_2O_3 (0001)/Cu (111) interface, Philosophical Magazine 85 (2005) 2961–2976.
[39] E.A. Jarvis, R.L. Hayes, E.A. Carter, Effects of oxidation on the nanoscale mechanisms of crack formation in aluminum, ChemPhysChem 2 (2001) 55–59.
[40] M. Cerny, J. Pokluda, On the effect of supercell size and strain localization in computational tensile tests, Modelling and Simulation in Materials Science and Engineering (2020).